Optimization and Evaluation of Torque-Sharing Functions for Torque Ripple Minimization in Switched Reluctance Motor Drives

X. D. Xue, K. W. E. Cheng, *Senior Member, IEEE*, and S. L. Ho

***Abstract*—Two improved torque-sharing functions for implementing torque ripple minimization (TRM) control are presented in this paper. The proposed torque-sharing functions are dependent on the turn-on angle, overlap angle, and the expected torque. This study shows that for a given torque the turn-on angle and the overlap angle have significant effects upon speed range, maximum speed, copper loss, and efficiency. Hence, genetic algorithm is used to optimize the turn-on angle and the overlap angle at various expected torque demands operating under the proposed TRM control in order to maximize the speed range and minimize the copper loss. Furthermore, four torque-sharing functions are used to derive the optimized results. At the same time, a fast and accurate online approach to compute the optimal turn-on and overlap angles is proposed. Therefore, this paper provides a valuable method to improve the performances of switched reluctance motor drives operating under TRM control.**

***Index Terms*—Genetic algorithm (GA), optimization, switched reluctance motor (SRM) drives, torque control, torque ripple minimization (TRM), torque-sharing function (TSF).**

I. Introduction

TORQUE-SHARING function (TSF) is an effective approach to implement the control of torque ripple minimization (TRM) in switched reluctance motor (SRM) drives [1]–[7]. In order to realize minimum torque ripples, it is shown that the proposed TSFs can be employed to distribute, intelligently, the reference torque among all the phases of the motor, while ensuring that the sum of all the individual phase torques is equal to the expected torque.

The choice of TSFs is not unique, and many functions satisfy the requirement of TRM control. Previously developed TSFs can be classified as either linear or nonlinear. The former means that the torque produced by a phase winding changes with the rotor position linearly, whereas the latter means that the torque produced by a phase winding changes nonlinearly with the rotor position. An early effort to develop exponential TSF for minimizing torque ripple was made by Illic-Spong *et al.* [1], and those functions are referred as m-functions. Schramm *et al.* [2] present a scheme of the linear TSF in which the torque changes linearly during phase commutation and the currents in two adjacent phases are the same at the central commutation point. At the same time, they also try to obtain the highest torque to current ratio [2]. Husain and Ehsani develop a sinusoidal TSF to implement TRM in SRM drives [3]. The cubic TSF is used in [4]–[6] in attempts to develop a smooth function. The torques produced by two phases during phase commutation change with the rotor position according to a cubic polynomial.

With the exception of attempts trying to realize the highest torque to current ratio [2], the effects of TSFs on other performance indicators of SRM drives have not been taken into account when these TSFs were used to implement TRM. On the contrary, this study is specifically addressing this issue.

The organization of this paper is described as follows. First, the authors will develop improved exponential and sinusoidal TSFs based on [1] and [3], and describe linear and cubic TSFs in Section II. The two criteria to evaluate TSFs will be proposed in Section III. Next, the effects of four TSFs on the speed range and the copper loss will be discussed in Section IV. In Section V, genetic algorithm (GA) is utilized to evaluate and optimize four TSFs for the maximization of speed range and minimization of copper loss, and the optimization function with two objectives will be developed. Then, the optimization of four TSFs will be discussed in Section VI. After that, four TSFs will be evaluated from the optimized results in Section VII. In Section VIII, an analytical model is proposed to compute, in real time, the optimal TSFs under TRM control. In addition, the applications of the proposed TSFs will be shown. Finally, the conclusions will be given in Section IX.

II. Torque-Sharing Functions

In order to minimize torque ripple in SRM drives using TSFs, torque/flux/current controllers have to be used to track the expected torque/flux/current value as governed by the TSFs. With this arrangement, the SRM drives operate under torque/flux/current hysteresis control or torque/flux/current pulsewidth modulation (PWM) control. TSFs are not suitable for the voltage single-pulse mode. The proposed commutation scheme for TSFs satisfies the following rules: 1) each phase winding produces only positive (motoring) torque and 2) at any time, only one phase winding or two adjacent phase windings are energized. Consequently, it can be deduced that the conduction angle (difference between the turn-off angle and the turn-on angle) is a constant for the specified SRM drives. For instance, the conduction angle must be 15° for all four-phase SRM drives.

Manuscript received May 19, 2008; revised September 18, 2008, December 1, 2008, and January 30, 2009. Current version published August 21, 2009. This work was supported by the Research Committee of the Hong Kong Polytechnic University under the Project G-YX52. Recommended for publication by Associate Editor J. Hur.

The authors are with the Department of Electrical Engineering, the Hong Kong Polytechnic University, Kowloon, Hong Kong (e-mail: eexdxue@polyu.edu.hk; eeecheng@polyu.edu.hk; eeslho@polyu.edu.hk).

Color versions of one or more of the figures in this paper are available online at http://ieeexplore.ieee.org.

Digital Object Identifier 10.1109/TPEL.2009.2019581

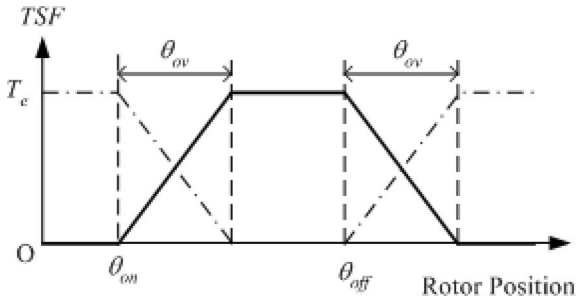

Fig. 1. Typical profile of the linear TSF.

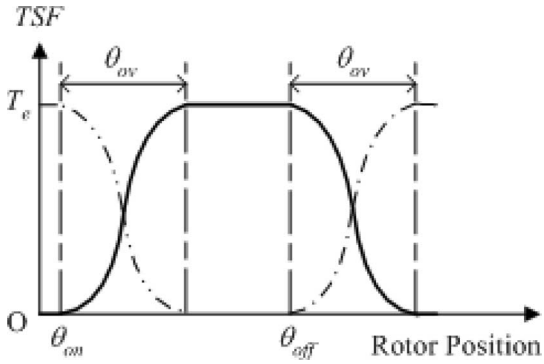

Fig. 2. Typical profile of the nonlinear TSF.

There is phase mutual coupling in SRM drives. Comparing with phase self-coupling, phase mutual coupling is quite small. Consequently, reported theoretical and simulation studies on TSFs neglected the effect of phase mutual coupling [1]–[7]. In real applications of TSFs, however, the measurement of phase current includes the effect of phase mutual coupling. The experimental results have verified that TSFs can be used to successfully implement TRM in SRM drives [1]–[6]. Thus, the theoretical and simulation studies without considering phase mutual coupling are reasonable.

A. Linear TSF

Linear TSF means that the torque produced by the phase in issue during phase commutation is changing linearly with the rotor position. A phase commutation scheme is presented in [2], where the torque is changing with the rotor position linearly during the overlapping conducting period of the two phases. Fig. 1 shows the typical profile of the linear TSF in which $\theta_{\rm on}$ denotes the turn-on angle, $\theta_{\rm ov}$ denotes the overlap angle, $\theta_{\rm off}$ denotes the turn-off angle, and T_e denotes the expected torque produced by the SRM.

For the rotor period in issue, the linear TSF can be defined by

$$\mathrm{TSF}(\theta)=\begin{cases}0, & (0\le\theta\le\theta_{\rm on})\\ f^l_{\rm up}(\theta), & (\theta_{\rm on}\le\theta\le\theta_{\rm on}+\theta_{\rm ov})\\ T_e, & (\theta_{\rm on}+\theta_{\rm ov}\le\theta\le\theta_{\rm off})\\ f^l_{\rm dn}(\theta), & (\theta_{\rm off}\le\theta\le\theta_{\rm off}+\theta_{\rm ov})\\ 0, & (\theta_{\rm off}+\theta_{\rm ov}\le\theta\le\theta_p)\end{cases}\tag{1}$$

where θ denotes the rotor position, θ_p denotes the rotor period, and $f^l_{\rm up}(\theta)$ and $f^l_{\rm dn}(\theta)$, respectively, denote the rising portion and the declining portion in the linear TSF.

From the control scheme, the overlap angle must meet

$$\theta_{\rm ov}\le\frac{\theta_p}{2}-\theta_{\rm off}.\tag{2}$$

From Fig. 1, the rising portion $f^l_{\rm up}(\theta)$ can be expressed by

$$f^l_{\rm up}(\theta)=\frac{T_e}{\theta_{\rm ov}}(\theta-\theta_{\rm on}).\tag{3}$$

Consequently, the declining portion $f^l_{\rm dn}(\theta)$ can be computed from

$$f^l_{\rm dn}(\theta)=T_e-\frac{T_e}{\theta_{\rm ov}}(\theta-\theta_{\rm off}).\tag{4}$$

The phase corresponding to $f^l_{\rm up}$ is the incoming phase and the phase corresponding to $f^l_{\rm dn}$ is the outgoing phase. Thus, the incoming phase and the outgoing phase are active simultaneously during phase commutation. There is only one active phase when there is no commutation.

B. Cubic TSF

With cubic TSF, the torque produced by the phases during phase commutation is changing nonlinearly with the rotor position. This nonlinearity has the form of a cubic polynomial. The cubic TSF is developed in [4]–[6]. Fig. 2 shows a typical profile of the cubic TSF.

The cubic TSF with respect to the rotor position can be defined by the cubic segments and constants. Within a rotor period, the cubic TSF can be expressed by [4]–[6]

$$\mathrm{TSF}(\theta)=\begin{cases}0, & (0\le\theta\le\theta_{\rm on})\\ f^c_{\rm up}(\theta), & (\theta_{\rm on}\le\theta\le\theta_{\rm on}+\theta_{\rm ov})\\ T_e, & (\theta_{\rm on}+\theta_{\rm ov}\le\theta\le\theta_{\rm off})\\ f^c_{\rm dn}(\theta), & (\theta_{\rm off}\le\theta\le\theta_{\rm off}+\theta_{\rm ov})\\ 0, & (\theta_{\rm off}+\theta_{\rm ov}\le\theta\le\theta_p)\end{cases}\tag{5}$$

where $f^c_{\rm up}(\theta)$ and $f^c_{\rm dn}(\theta)$ represent the rising portion and the declining portion in the cubic TSF, respectively.

In the same way, the overlap angle must satisfy (2).

The rising portion $f^c_{\rm up}(\theta)$ is defined by the cubic segment and is computed from

$$f^c_{\rm up}(\theta)=u_0+u_1(\theta-\theta_{\rm on})+u_2(\theta-\theta_{\rm on})^2+u_3(\theta-\theta_{\rm on})^3.\tag{6}$$

Furthermore, $f^c_{\rm up}(\theta)$ must satisfy the constraints which are

$$f^c_{\rm up}(\theta)=\begin{cases}0, & (\theta=\theta_{\rm on})\\ T_e, & (\theta=\theta_{\rm on}+\theta_{\rm ov})\end{cases}\tag{7}$$

and

$$\frac{df^c_{\rm up}(\theta)}{d\theta}=\begin{cases}0, & (\theta=\theta_{\rm on})\\ 0, & (\theta=\theta_{\rm on}+\theta_{\rm ov}).\end{cases}\tag{8}$$

Hence, the coefficients in the expression ($f_{\rm up}^{c}(\theta)$) can be computed from (7) and (8). The computed results are given by

$$\begin{cases} u_0 = 0 \\ u_1 = 0 \\ u_2 = \dfrac{3T_e}{\theta_{\rm ov}^2} \\ u_3 = \dfrac{-2T_e}{\theta_{\rm ov}^3}. \end{cases} \tag{9}$$

Consequently, (6) is simplified to

$$f_{\rm up}^{c}(\theta) = \frac{3T_e}{\theta_{\rm ov}^2}(\theta - \theta_{\rm on})^2 - \frac{2T_e}{\theta_{\rm ov}^3}(\theta - \theta_{\rm on})^3. \tag{10}$$

Thus, the declining portion $f_{\rm dn}^{c}(\theta)$ can be computed from

$$f_{\rm dn}^{c}(\theta) = T_e - f_{\rm up}^{c}(\theta - \theta_{\rm off} + \theta_{\rm on}). \tag{11}$$

C. Sinusoidal TSF

With sinusoidal TSF, the torque produced by the phases during phase commutation is changing with the rotor position in accordance to a sinusoidal function. Husain and Ehsani [3] present a sinusoidal TSF. The typical profile of the sinusoidal TSF is similar to that in Fig. 2. Within a rotor period, the sinusoidal TSF proposed in this paper is expressed by

$$\mathrm{TSF}(\theta) = \begin{cases} 0, & (0 \le \theta \le \theta_{\rm on}) \\ f_{\rm up}^{s}(\theta), & (\theta_{\rm on} \le \theta \le \theta_{\rm on} + \theta_{\rm ov}) \\ T_e, & (\theta_{\rm on} + \theta_{\rm ov} \le \theta \le \theta_{\rm off}) \\ f_{\rm dn}^{s}(\theta), & (\theta_{\rm off} \le \theta \le \theta_{\rm off} + \theta_{\rm ov}) \\ 0, & (\theta_{\rm off} + \theta_{\rm ov} \le \theta \le \theta_p) \end{cases} \tag{12}$$

where $f_{\rm up}^{s}(\theta)$ and $f_{\rm dn}^{s}(\theta)$ represent the rising portion and the declining portion in the sinusoidal TSF, respectively.

In the same way, the overlap angle must satisfy (2).

The sinusoidal TSF developed in [3] is only the function of the turn-on and turn-off angles. In this paper, the sinusoidal TSF in [3] is improved. The improved sinusoidal TSF depends on the turn-on, turn-off, and overlap angles. The improved rising portion $f_{\rm up}^{s}(\theta)$ is determined by

$$f_{\rm up}^{s}(\theta) = \frac{T_e}{2} - \frac{T_e}{2}\cos\frac{\pi}{\theta_{\rm ov}}(\theta - \theta_{\rm on}). \tag{13}$$

Similarly, the improved declining portion $f_{\rm dn}^{s}(\theta)$ is computed from

$$f_{\rm dn}^{s}(\theta) = \frac{T_e}{2} + \frac{T_e}{2}\cos\frac{\pi}{\theta_{\rm ov}}(\theta - \theta_{\rm off}). \tag{14}$$

D. Exponential TSF

For exponential TSF, the torque produced by the phases during phase commutation changes with rotor position with exponential functions. An exponential TSF is presented in [1]. For the exponential TSF, the rising portion and the declining portion are not symmetrical about the middle position. Furthermore, the exponential TSF in [1] depends only on the turn-on angle. Referring to Fig. 2, in this study, the improved exponential TSF is defined by

$$\mathrm{TSF}(\theta) = \begin{cases} 0, & (0 \le \theta \le \theta_{\rm on}) \\ f_{\rm up}^{e}(\theta), & (\theta_{\rm on} \le \theta < \theta_{\rm on} + \theta_{\rm ov}) \\ T_e, & (\theta_{\rm on} + \theta_{\rm ov} \le \theta \le \theta_{\rm off}) \\ f_{\rm dn}^{e}(\theta), & (\theta_{\rm off} \le \theta < \theta_{\rm off} + \theta_{\rm ov}) \\ 0, & (\theta_{\rm off} + \theta_{\rm ov} \le \theta \le \theta_p) \end{cases} \tag{15}$$

where $f_{\rm up}^{e}(\theta)$ and $f_{\rm dn}^{e}(\theta)$ represent the rising portion and the declining portion in the exponential TSF, respectively.

The rising portion $f_{\rm up}^{e}(\theta)$ is expressed by

$$f_{\rm up}^{e}(\theta) = T_e\left[1 - \exp\left(\frac{-(\theta - \theta_{\rm on})^2}{\theta_{\rm ov}}\right)\right]. \tag{16}$$

The declining portion $f_{\rm dn}^{e}(\theta)$ is given by

$$f_{\rm dn}^{e}(\theta) = T_e\left[\exp\left(\frac{-(\theta - \theta_{\rm off})^2}{\theta_{\rm ov}}\right)\right]. \tag{17}$$

E. Cases of Four TSFs

This evaluation is implemented using the electronic control approach. The TSFs are dependent on the turn-on angle, the overlap angle, and the expected torque. However, a change in the numbers of stator and rotor teeth will result in variations in the turn-on angle and the overlap angle in TRM optimization. In other words, variations in design parameters of an SRM have no effect on the effectiveness of this algorithm if the numbers of stator and rotor teeth do not change; otherwise, modifications in the control algorithm are necessary. Fig. 3 shows the typical profiles of the aforementioned four TSFs for a four-phase SRM drive with its main parameters described in the Appendix. In Fig. 3, the turn-on angle is 5°, the overlap angle is 5°, the turn-off angle is 20°, and the expected torque is 2 Nm. The top to bottom profiles in each of the figures in Fig. 3(a)–(d) are the torque reference, flux linkage reference, current reference, and rate-of-change of the flux linkage with respect to the position, respectively.

III. Evaluation Criteria

Clearly, the purpose of developing TSFs is to minimize torque ripple. On the other hand, the actual torque output is dependent on whether or not the current or flux linkage controller can accurately track the current or flux linkage references generated by TSFs. In general, good tracking ability implies that saturation does not appear in the current or flux linkage controller. This means the required voltage must be lower than the available dc-link voltage. In other words, the current or flux linkage reference should be as smooth as possible to avoid the current or flux linkage controller from going into saturation. The rate-of-change of the current or flux linkage reference is thus expected to be as small as possible. This is the most basic and crucial requirement on TSFs. At the same time, minimum rate-of-change of the current or flux linkage reference implies that the drive is operating with its maximum speed range for a given dc-link voltage. The rate-of-change of either the current or the flux linkage may be selected to evaluate the TSFs.

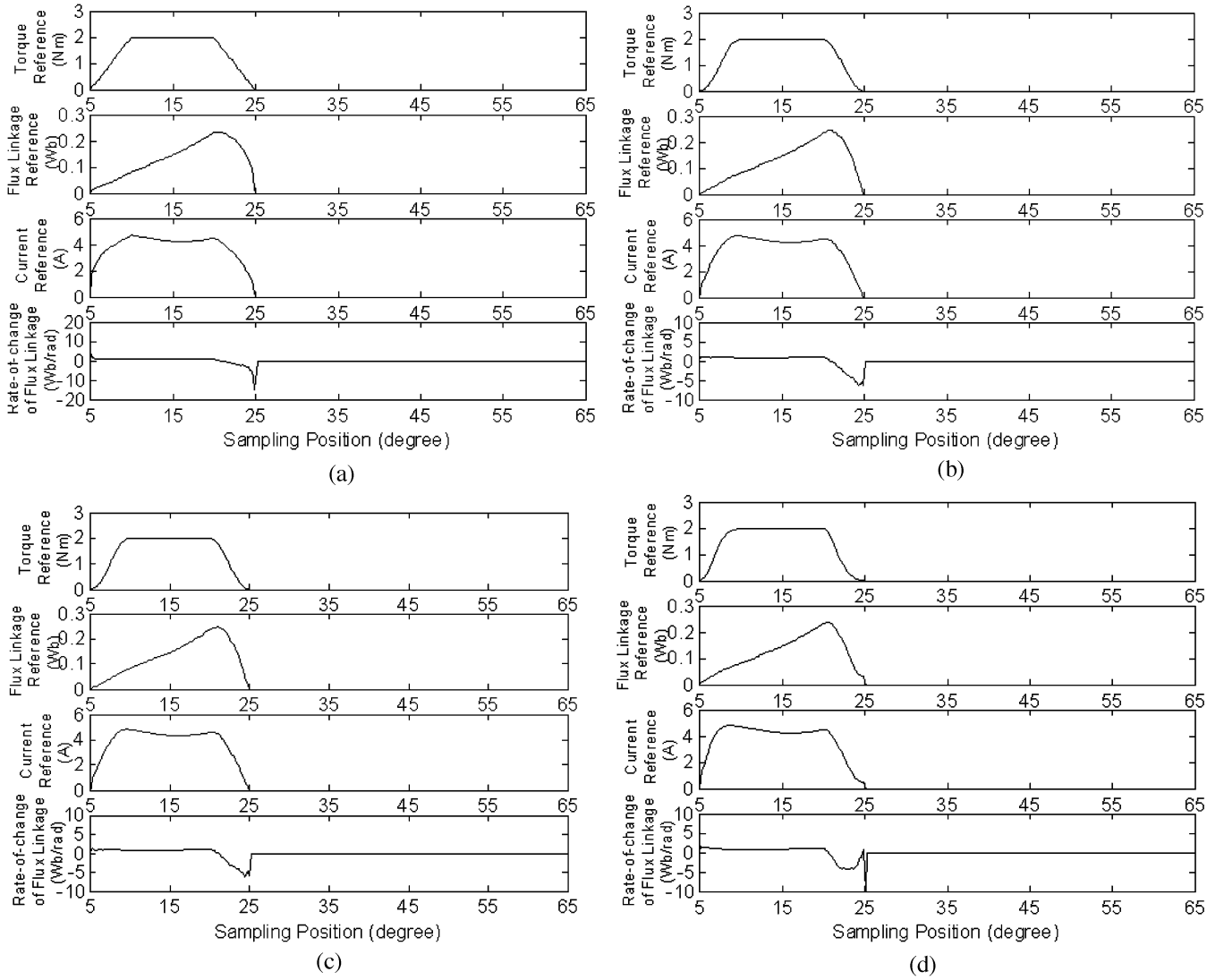

Fig. 3. Waveforms of four types of TSFs. (a) Linear TSF. (b) Cubic TSF. (c) Sinusoidal TSF. (d) Exponential TSF.

A. *Rate-of-Change of Flux Linkage*

Neglecting mutual coupling between the phase windings and selecting the flux linkage as the controlled variable, it is well known that the rate-of-change of the flux linkage in SRM drives is determined by

$$\frac{d\psi}{dt} = V - ir \tag{18}$$

where ψ represents the flux linkage, t is the time, V is the voltage applied to the phase windings, i is the phase current, and r is the resistance of the phase windings.

At steady state and in the case of nonzero speed, (18) can be changed into

$$\frac{d\psi}{d\theta} = \frac{V - ir}{\omega} \tag{19}$$

where ω is the motor speed.

In general, the ohmic voltage drop is very small compared to the dc-link voltage. Hence, neglecting the ohmic voltage drop, (19) can be simplified to

$$\frac{d\psi}{d\theta} = \frac{V}{\omega}. \tag{20}$$

Neglecting the on-state voltage drop of the switching components, the voltage applied to the phase windings is the dc-link voltage. It is clear that the rate-of-change of the flux linkage with respect to the position is dependent on the dc-link voltage and motor speed. The effect of current upon the change in flux linkage is much weaker. The flux linkage varies approximately linearly with the position at constant voltage and speed. Consequently, the computation of the allowable maximum rate-of-change of the flux linkage for a given dc-link voltage and speed is simple and fast. Xue and Cheng [7] show that a flux linkage hysteresis controller with a cubic TSF can be used to implement TRM control.

B. Rate-of-Change of Current

From (19), the rate-of-change of the current with respect to the position can be derived as

$$\frac{di}{d\theta} = \frac{V - ir - \omega \partial\psi/\partial\theta}{\omega \partial\psi/\partial i}. \tag{21}$$

The rate-of-change of the current with respect to position is a highly nonlinear function even at constant voltage and speed. Such nonlinearity makes it complicated and difficult to compute the allowed maximum rate-of-change of the current for a given dc-link voltage and speed.

From the previous analysis, it can be seen that the use of flux linkage is better than current in the determination of the operating limits of the controller. Hence, flux linkage controller is studied in this paper.

C. Evaluation Criteria

Two optimization criteria are proposed. Both are for the minimization of copper loss and maximization of speed range. The rate-of-change of the flux linkage at the $(k+1)$th sampling position is computed from

$$\left(\frac{d\psi}{d\theta}\right)_{k+1} = \frac{\psi_{k+1} - \psi_k}{\theta_{k+1} - \theta_k} \tag{22}$$

where θ_k represents the kth sampling position and ψ_k represents the flux linkage reference with respect to θ_k.

For the specified turn-on angle, overlap angle, and expected torque, a TSF can be determined, and hence, a torque reference profile is generated. From the determined torque reference profile, the current profile is determined using the given torque characteristics. Consequently, the flux linkage profile is computed from the current profile using the given flux linkage characteristics. At each sampling position on the flux linkage reference profile, there is a rate-of-change of the flux linkage. Among these rates-of-change of the flux linkage, the maximum rate-of-change of the flux linkage is denoted as the effective rate-of-change of the flux linkage corresponding to this TSF. The effective rate-of-change of the flux linkage for a TSF is expressed by

$$R_\psi^e = \left(\frac{d\psi}{d\theta}\right)^e = \max_{k=0,1,\ldots,(N_s-1)} \left\{ \left| \left(\frac{d\psi}{d\theta}\right)_{k+1} \right| \right\} \tag{23}$$

where N_s represents the number of sampling positions.

Therefore, the first parameter to evaluate TSFs is the effective rate-of-change of the flux linkage in this study. For various turn-on angles, overlap angles, and expected torques, there are different effective rates-of-change of flux linkage. From Fig. 3(a)–(d), the effective rates-of-change of the flux linkage are 15.0921, 6.1610, 6.0990, and 9.9981 Wb/rad, respectively.

In order to accurately track the flux linkage reference online for the proposed TRM control, the maximum effective rate-of-change of the flux linkage must satisfy

$$\left(\frac{d\psi}{d\theta}\right)^e_{\max} \le \frac{V_{\rm dc}}{\omega_{\max}} \tag{24}$$

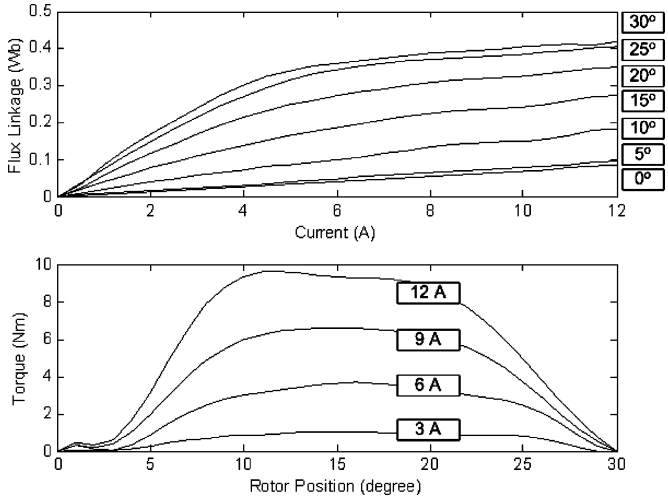

Fig. 4. Given flux linkage and static torque characteristics.

where $V_{\rm dc}$ is thedc-link voltage and $\omega_{\max}$ is the maximum motor speed.

It can be seen from (24) that the maximum effective rate-of-change of the flux linkage governs also the maximum speed or the speed range. To be specific, the smaller the maximum effective rate-of-change of the flux linkage, the larger the maximum speed. For the given dc-link voltage, hence, the maximum speed is inversely proportional to the maximum effective rate-of-change of the flux linkage approximately.

Total losses in an SRM should be used to evaluate TSFs. The total losses can be regarded as the sum of the iron loss and copper loss. For the specified dc-link voltage and motor speed, the variation in the total losses mainly depends on the copper loss. Thus, the second parameter selected in this study is the copper loss. It can be expressed by the square of the rms current, which is computed from

$$I_{\rm rms}^2 = \frac{\int_{\theta_{\rm on}}^{(\theta_{\rm on}+\theta_p)} i^2 d\theta}{\theta_p}. \tag{25}$$

IV. Effects of TSFs

A four-phase SRM drive is utilized to evaluate the aforementioned four TSFs. The main parameters of the prototype are given in the Appendix. One complete period of the flux linkage is 60° for the four-phase SRM. The rotor position is equal to 0° when the stator pole is fully unaligned with the rotor pole. The rotor position is equal to half of the rotor period (30° for a four-phase SRM drive) when the stator pole is completely aligned with the rotor pole. The magnetic characteristics and static torque characteristics of the prototype are illustrated in Fig. 4 [8]–[10]. These characteristics are utilized to evaluate quality of the four TSFs. In addition, the sampling step size has a fixed value that is selected as 0.2° in this paper in order to eliminate the effect of the motor speed on the sampling positions. In the computation, analytical flux linkage estimator and analytical torque estimator are used [8]–[10]. 2-D least-square estimators are employed in this paper [8].

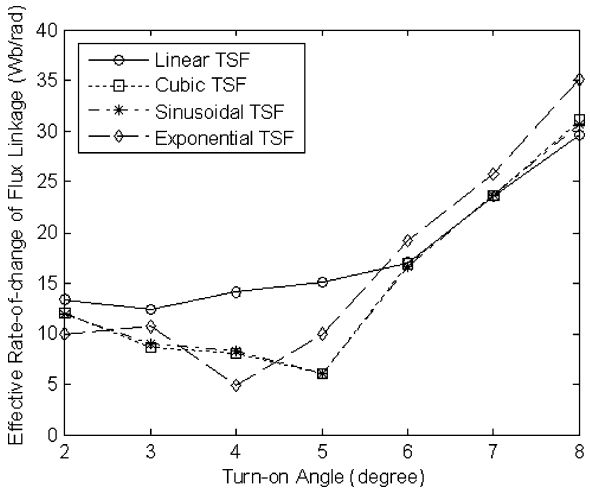

Fig. 5. Effects of the turn-on angle on the effective rate-of-change of the flux linkage.

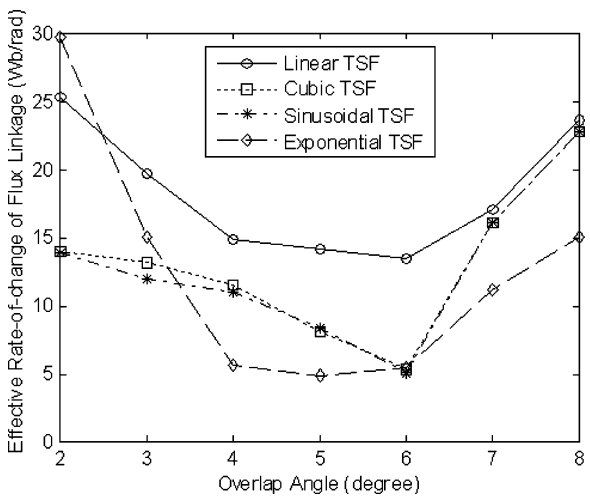

Fig. 6. Effects of the overlap angle on the effective rate-of-change of the flux linkage.

A. *Effective Rate-of-Change of Flux Linkage*

In this section, the effective rate-of-change of the flux linkage is used to evaluate the four TSFs. Good implementation of TRM and the motor speed range are dependent on the effective rate-of-change of the flux linkage. Fig. 5 shows the effective rate-of-change of the flux linkage versus the turn-on angle, with the overlap angle being set to 5° and the expected torque being 2 Nm.

It can be observed from Fig. 5 that the turn-on angle has a considerable bearing upon the effective rate-of-change of the flux linkage. For any one of four TSFs, the minimum value of the effective rate-of-change of the flux linkage can be found by optimizing the turn-on angle for the given overlap angle and expected torque. The cubic TSF and the sinusoidal TSF have roughly the same effective rate-of-change of flux linkage.

When the turn-on angle equals to 4° and the expected torque is 2 Nm, the effects of the overlap angle on the effective rate-of-change of the flux linkage are illustrated in Fig. 6.

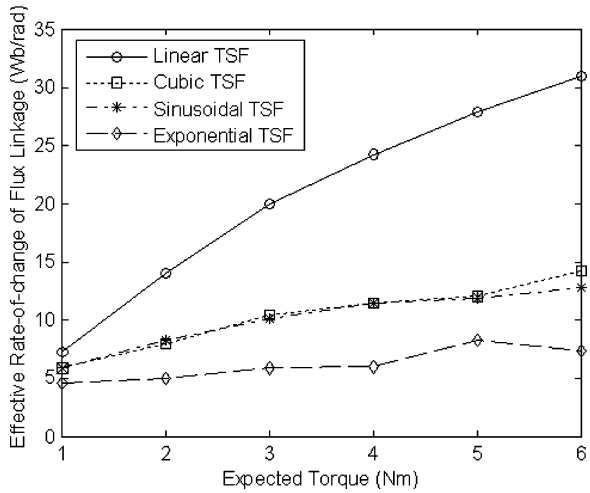

Fig. 7. Effects of the expected torque on the effective rate-of-change of the flux linkage.

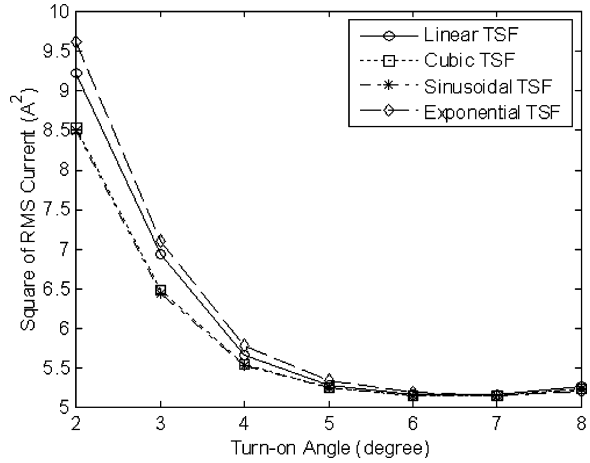

Fig. 8. Effects of the turn-on angle on the copper loss.

It is clear that the overlap angle also has a significant effect on the effective rate-of-change of the flux linkage. The linear TSF results in a larger effective rate-of-change of the flux linkage than those of the other three nonlinear TSFs having various overlap angles. In the same way, the minimum value of the effective rate-of-change can be obtained by optimizing the overlap angle for specific turn-on angle and expected torque.

The effects of variations in the expected torque upon the effective rate-of-change of the flux linkage can be seen in Fig. 7, where the turn-on angle is 4° and the overlap angle is 5°. It is clear that the effective rate-of-change of the flux linkage goes up with increases in the expected torque for the four TSFs.

B. *Copper Loss*

When the turn-on angle changes, the variation in the square of the rms current is shown in Fig. 8, where the overlap angle is 5° and the expected torque is 2 Nm. It can be seen that the turn-on angle has a strong bearing on the square of the rms current. By optimizing the turn-on angle, the minimum copper loss can also be found for the specific overlap angle and

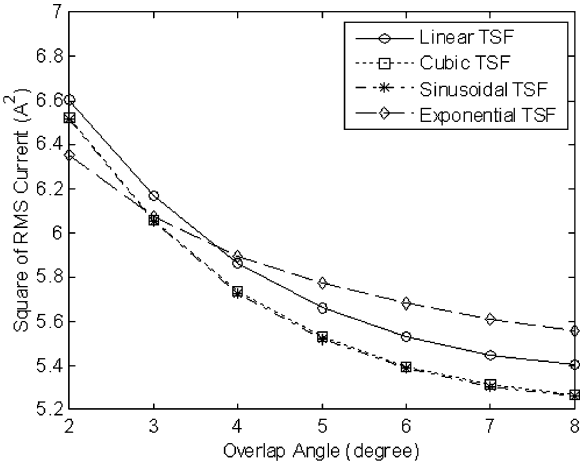

Fig. 9. Effects of the overlap angle on the copper loss.

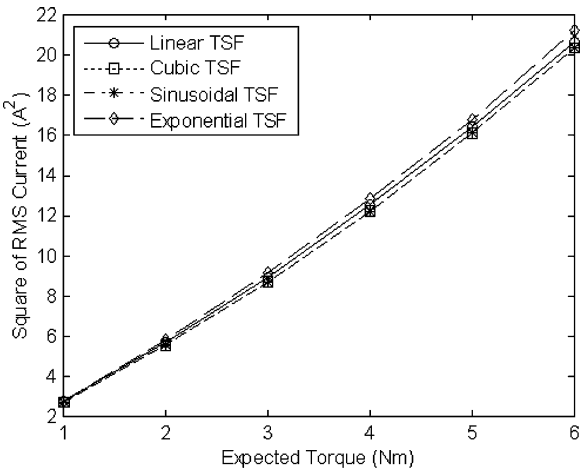

Fig. 10. Effects of the expected torque on the copper loss.

expected torque. The exponential TSF produces larger copper loss compared to those from the other three TSFs. The copper loss produced by the cubic TSF is almost the same as that from sinusoidal TSF. For all four TSFs, the minimum copper losses can be found by optimizing the turn-on angle.

The effects of the overlap angle on the square of the rms current are depicted in Fig. 9, where the turn-on angle is 4° and the expected torque is 2 Nm. Clearly, the overlap angle has noticeable effects on the copper loss of all four TSFs. The increase in the overlap angle will lead to a reduction in copper loss. Moreover, the cubic TSF and the sinusoidal TSF produce the same copper loss approximately.

Fig. 10 shows the change in the square of the rms current with the expected torque for a turn-on angle of 4° and an overlap angle of 5°. Obviously, the copper loss will go up if the expected torque increases.

V. Fitness Function

A. Optimized Parameters

It can be seen from the evaluations of four TSFs in the last section that the effective rate-of-change of the flux linkage and the copper loss are dependent on both the turn-on angle and the overlap angle for a specific torque. Furthermore, the local minimum value of the effective rate-of-change of the flux linkage and the local minimum copper loss for a given torque can be obtained by optimizing the turn-on angle and the overlap angle. Therefore, the turn-on angle and the overlap angle are selected as the optimized variables in this paper in order to identify the global minimum value of the effective rates-of-change of the flux linkage or the global minimum value of the copper losses. For the prototype of the four-phase SRM drive, TSFs are symmetrical about the position of 15°. Consequently, the sum of the turn-on angle and the overlap angle must be less than 15°. Considering the effects of the turn-on angle and the overlap angle discussed in the Section IV, the range the turn-on angle is selected as the one from 3° to 6° and the range of the overlap angle is selected as the one from 4° to 8°.

B. Fitness Function

In this paper, two optimization objectives are selected. One of which is the effective rate-of-change of the flux linkage and the other is the square of the rms current. GA is used to optimize the turn-on angle and the overlap angle. The fitness function is composed of these two optimization objectives as

$$\text{FitnessFunction} = \min\left[w_f \bar{R}^e_\psi + (1 - w_f)\bar{I}^2_{\text{rms}}\right] \tag{26}$$

where w_f denotes the weight factor of the optimization objectives ($0 \le w_f \le 1$), and $\bar{R}^e_\psi$ and $\bar{I}^2_{\text{rms}}$ are, respectively, computed from

$$\bar{R}^e_\psi = \frac{R^e_\psi}{R^e_{\psi\,\max}} \tag{27}$$

and

$$\bar{I}^2_{\text{rms}} = \frac{I^2_{\text{rms}}}{I^2_{\text{rms}\,\max}} \tag{28}$$

where $R^e_{\psi\,\max}$ and $I^2_{\text{rms}\,\max}$ denote the maximum R^e_ψ and the maximum I^2_{rms}.

The proposed fitness function consists of two optimization objectives when $0 < w_f < 1$. The objective function comprises only the effective rate-of-change of the flux linkage when $w_f = 1$. The objective function includes just the square of the rms current when $w_f = 0$. Thus, the weight factor indicates the weightings taken up by the effective rate-of-change of the flux linkage or the square of the rms current.

VI. Optimization

A. Linear TSF

Fig. 11 shows the minimum effective rate-of-change of flux linkage and the minimum of the square of the rms current obtained from the linear TSF. It is clear that the best minimum effective rate-of-change of flux linkage and the worst minimum square of rms current can be obtained when the weight factor is 1.0. The best minimum square of rms current and the worst minimum effective rate-of-change of flux linkage are obtained when the weight factor is equal to zero. On the other hand, the

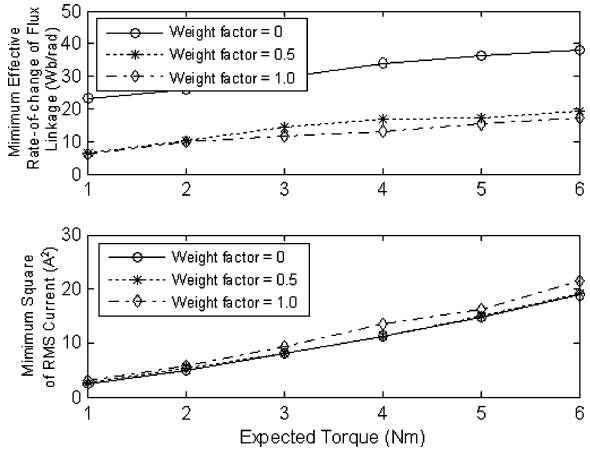

Fig. 11. Optimization of linear TSF.

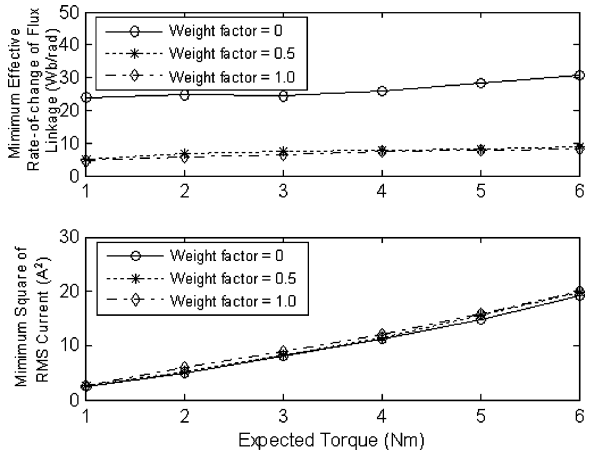

Fig. 12. Optimization of cubic TSF.

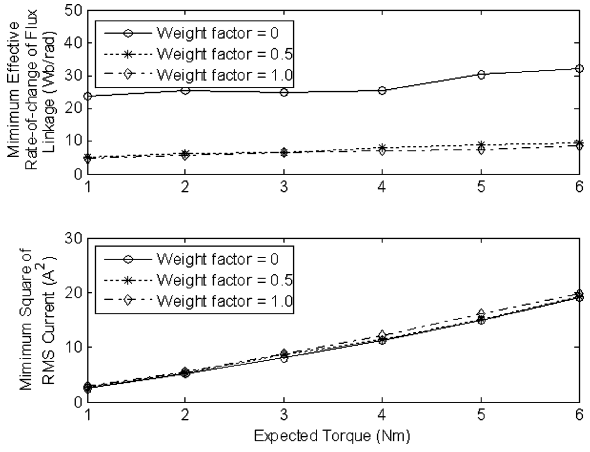

Fig. 13. Optimization of sinusoidal TSF.

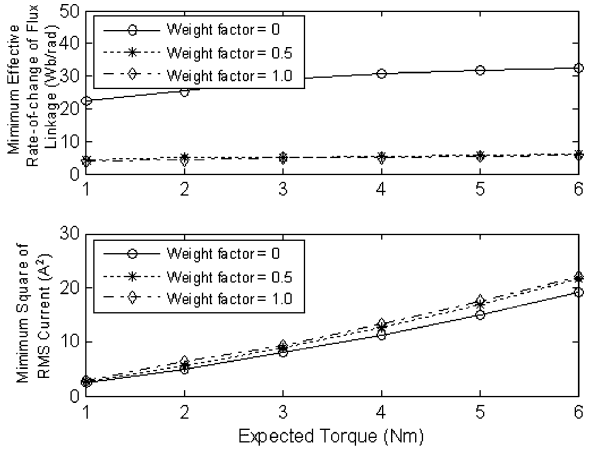

Fig. 14. Optimization of exponential TSF.

good minimum effective rate-of-change of flux linkage and the good minimum square of rms current are obtained when the weight factor is equal to 0.5.

B. Cubic TSF

The optimization results with cubic TSF are illustrated in Fig. 12. Similar to the linear TSF, if the weight factor is 1.0, the best minimum effective rate-of-change of flux linkage and the worst minimum square of rms current are obtained. If the weight factor is 0, the best minimum square of rms current and the worst minimum rate-of-change of flux linkage are obtained. If the weight factor is 0.5, both the good minimum effective rate-of-change of flux linkage and the good minimum square of the rms current are obtained simultaneously.

C. Sinusoidal TSF

For the sinusoidal TSF, the optimization results are depicted in Fig. 13. Obviously, the best minimum effective rate-of-change of flux linkage and the worst minimum square of rms current are produced if the weight factor is 1.0, while the best minimum square of rms current and the worst minimum effective rate-of-change of flux linkage are obtained if the weight factor is 0.

When the weight factor is 0.5, the good minimum effective rate-of-change of flux linkage and the good minimum square of rms current are obtained.

D. Exponential TSF

Fig. 14 depicts the optimization results of the exponential TSF. The analytical result similar to the aforementioned three TSFs can be obtained.

E. Weight Factor

The relationships between the minimum effective rate-of-change of flux linkage, and minimum square of rms current and the weight factor are illustrated in Figs. 15–18. The solid curves represent the minimum effective rate-of-change of flux linkage, and the dotted curves represent the minimum square of rms current.

It can be seen for any one of the four TSFs that the minimum square of rms current reaches to the minimum value if the weight factor is equal to 0, the minimum effective rate-of-change of flux linkage leads to the minimum value if the weight factor

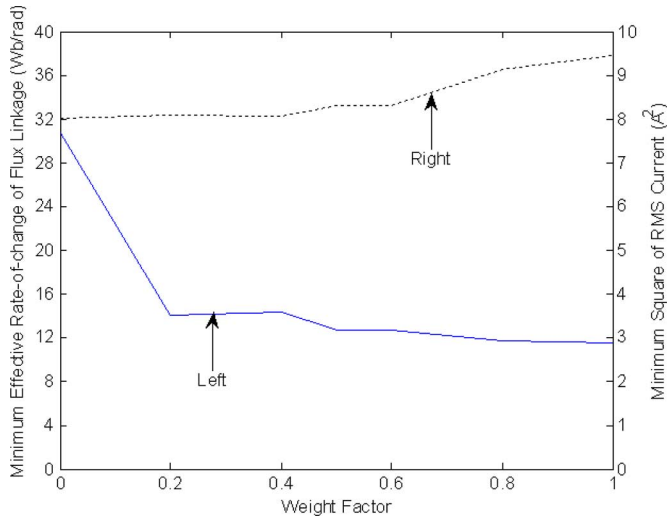

Fig. 15. Linear TSF.

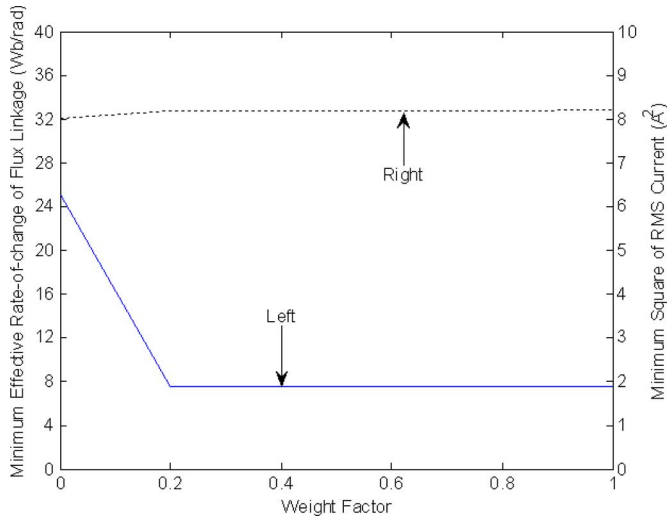

Fig. 16. Cubic TSF.

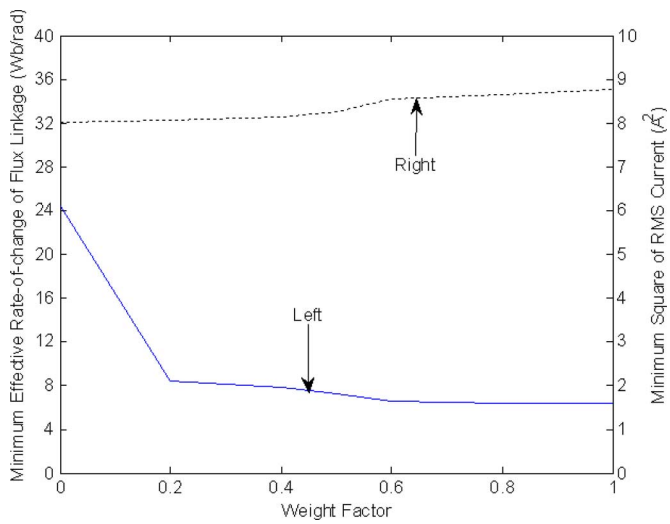

Fig. 17. Sinusoidal TSF.

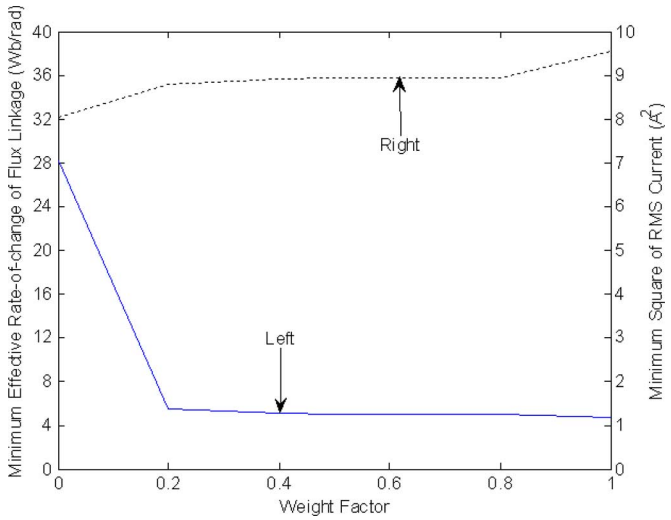

Fig. 18. Exponential TSF.

is equal to unity, and the minimum effective rate-of-change of flux linkage decreases and the minimum square of rms current increases if the weight factor becomes large. The result is easily understood. On the one hand, the optimization function includes only one objective that is to minimize the square of rms current (i.e., minimum copper loss) if the weight factor is selected as 0. On the other hand, the optimization function also includes one objective that is to minimize the effective rate-of-change of flux linkage (i.e., maximum speed range) if the weight factor is selected as unity.

Therefore, the weight factor should be selected as zero when designing TSFs in order to obtain only minimum copper loss. The weight factor should be selected as unity when designing TSFs in order to fulfill only maximum speed range. In order to obtain the correct balance between the maximum speed range and the minimum copper loss, generally, it is the reasonable choice that the weight factor is selected as 0.5.

In summary, it can be observed that for all the four TSFs, the weight factor has significant bearings on the minimum effective rate-of-change of flux linkage as well as on the minimum square of rms current. For each of the four TSFs, the square of rms current, and not effective rate-of-change of flux linkage, has the minimum value, when the weight factor is equal to zero. Conversely, the effective rate-of-change of the flux linkage, and not the square of rms current, has the minimum value, when the weight factor equals to unity. Both the small effective rate-of-change of flux linkage and the fairly small square of the rms current can be obtained when the weight factor is 0.5. Hence, the appropriate selection of the weight factor can result in both desirable speed range and small copper loss.

VII. Evaluation of Four TSFs

The aforementioned four TSFs can be used to implement TRM control in SRM drives. However, it is noted that a reasonable selection of TSFs will be highly instrumental for improving other performance indicators of SRM drives, such as speed range and efficiency.

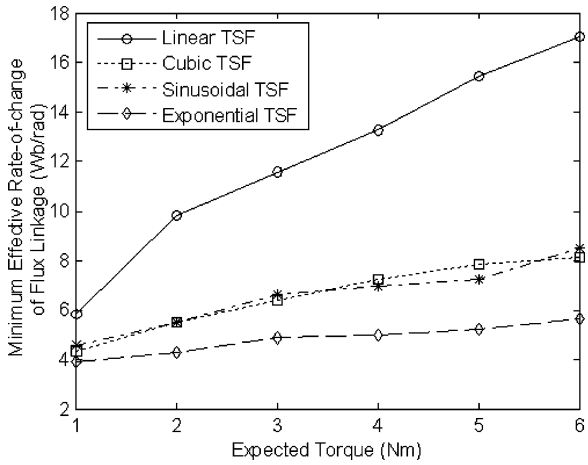

Fig. 19. Minimum effective rate-of-change of flux linkage at the weight factor of 1.0.

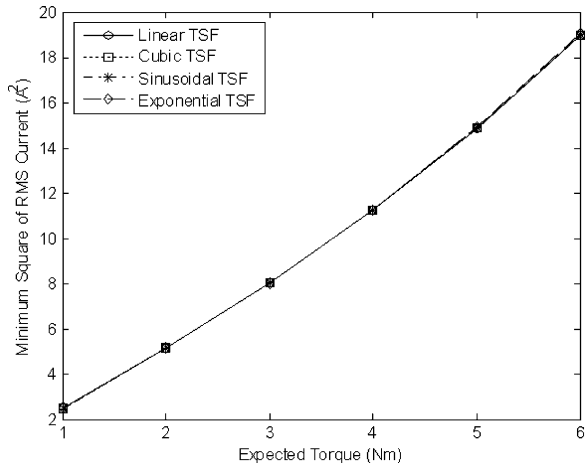

Fig. 20. Minimum square of rms current at the weight factor of 0.

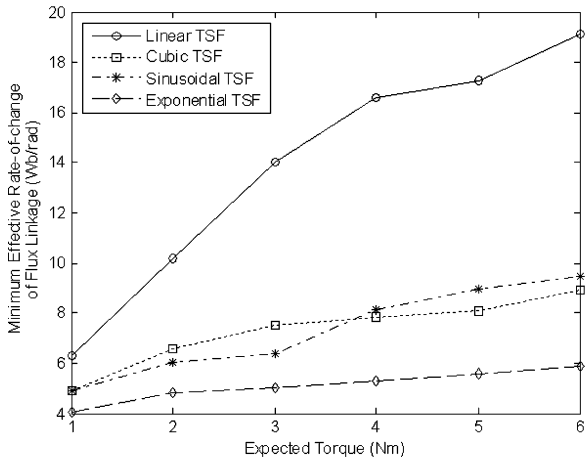

(a)

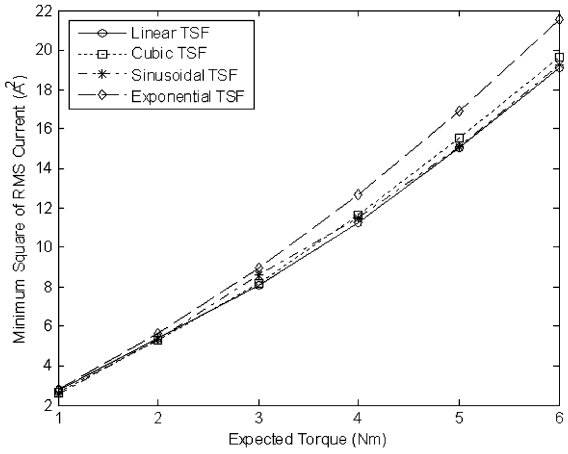

(b)

Fig. 21. Comparision between four TSFs at the weight factor of 0.5. (a) Minimum effective rate-of-change of flux linkage. (b) Minimum square of rms current.

A. Speed Range

When the weight factor is equal to 1.0, the fitness function includes only the minimum effective rate-of-change of flux linkage. Fig. 19 illustrates the minimum effective rates-of-change of the flux linkage by optimizing the turn-on and overlap angles when the weight factor is unity. It can be observed that the minimum effective rates-of-change of flux linkage from the linear TSF are much larger than the ones obtained from other three TSFs. The minimum effective rates-of-change of flux linkage from the cubic and sinusoidal TSFs are appropriately the same, and the minimum effective rates-of-change of flux linkage from the exponential TSF are much smaller than those obtained from other three TSFs. If the maximum speed of SRM drives with the TRM control is only regarded as the evaluating target, the exponential TSF is the best selection among four TSFs. The second best selection for the aforementioned target is either the cubic or sinusoidal TSF.

B. Minimum Copper Loss

The fitness function is the minimum square of the rms current when the weight factor is 0. Fig. 20 illustrates the optimization results when $w_f = 0$. It is clear that the minimum rms current from four TSFs is approximately the same. In other words, if only the minimum copper loss is being taken into account, any TSF among the four may be used.

C. Speed Range and Copper Loss

In general, both large speed range and small copper loss are sought. When the weight factor is larger than 0 and smaller than 1.0, the proposed fitness function includes two optimization objectives, which are the minimum effective rate-of-change of flux linkage (governing the speed range) and the minimum square of the rms current (governing the copper loss). Fig. 21(a) shows a comparison of the minimum effective rates-of-change of flux linkage between four TSFs, and Fig. 21(b) shows the comparison of the minimum square of rms current between the four TSFs when the weight factor is 0.5. Obviously, the linear TSF is not a good selection because its minimum effective rates-of-change of flux linkage are much larger than those obtained from other three TSFs. The cubic TSF and the sinusoidal TSF have almost the same minimum effective rate-of-change of flux linkage and the same minimum square of rms current. The exponential TSF

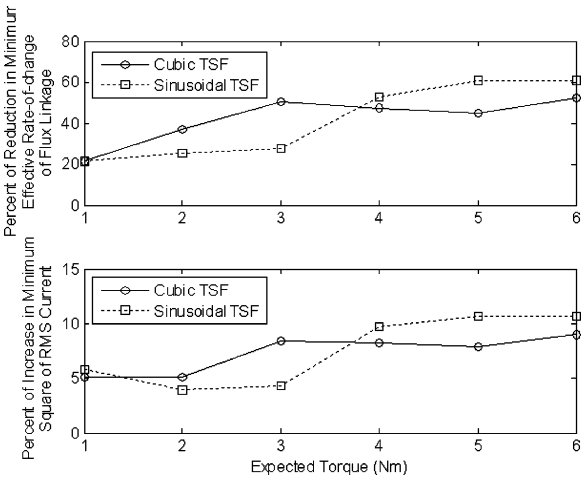

Fig. 22. Comparison of the exponential TSF with the cubic and sinusoidal TSFs at the weight factor of 0.5.

has better minimum effective rate-of-change of flux linkage and worse minimum square of rms current when compared to those obtained using cubic or sinusoidal TSF.

Comparing the minimum effective rates-of-change of flux linkage from the exponential TSF with the ones obtained from cubic and sinusoidal TSFs, the reduction percentage is illustrated in the top graph of Fig. 22. In the same way, comparing the minimum squares of rms current from the exponential TSF with those obtained from cubic and sinusoidal TSFs, the bottom graph in Fig. 22 shows the percentage of increase. It can be observed that the minimum effective rate-of-change of flux linkage from the exponential TSF is smaller than those obtained from cubic or sinusoidal TSF, and the percentage of reduction is over 20%. However, the minimum square of rms current from the former is larger than those obtained from the latter, and the percentage of increase is less than 10%. Thus, the reduction of the minimum effective rate-of-change of flux linkage is much larger than increases in the minimum square of rms current. Hence, the exponential TSF is a reasonable selection for improving both speed range and efficiency using TRM control. However, if the minimum effective rate-of-change of flux linkage from the cubic or sinusoidal TSF can satisfy the demand on the speed range, the cubic or sinusoidal TSF should be the preferred selection.

VIII. Actual Optimal Turn-on Angle and Overlap Angle

In the actual TRM control, it is important to obtain the actual optimal turn-on angle and overlap angle simply and quickly. The aforementioned studies have shown that the optimal turn-on angles and overlap angles are changing with the expected torque. Hence, it is suggested that the analytical least-square polynomials are used to match the optimal turn-on angles and the optimal overlap angles. The proposed

TABLE I
Least-Square Coefficients for Exponential TSF when $w_f = 1.0$

Coefficient c_k	Optimal turn-on angle	Optimal overlap angle
c_0	0.366838E+01	0.534111E+01
c_1	0.193509E+00	-0.344386E+00
c_2	-0.140883E+00	0.416923E+00
c_3	-0.339762E-01	-0.504979E-01
c_4	0.180773E-01	-0.581607E-01
c_5	0.114940E-02	0.136477E-01

least-square polynomial can be expressed by

$$\theta(T_e) = \sum_{k=0}^{N_{\rm ls}} c_k (T_e - \bar{T}_e)^k \tag{29}$$

$$\bar{T}_e = \frac{\sum_{j=0}^{N_e-1} T_{ej}}{N_e} \tag{30}$$

where θ may be the turn-on angle or the overlap angle, c_k represents the least-square coefficients determined by either the given optimal turn-on or overlap angles, $N_{\rm ls}$ represents the number of the least-square coefficients, N_e represents the number of the given torque, and T_{ej} represents the given torque.

A. Weight Factor = 1

From the previous analyses, the fitness function is composed only of the effective rate-of-change of flux linkage if the weight factor is 1.0. Thus, the exponential TSF is the prior selection. Consequently, the least-square coefficients for the optimal turn-on or overlap angles can be computed from the given optimal turn-on or overlap angles, which are obtained from the GA optimization in the last section. Table I shows the least-square coefficients for the exponential TSF when $N_{\rm ls}$ is equal to 6. Using the proposed analytical expression, the computed optimal turn-on and overlap angles, and the given optimal turn-on and overlap angles are depicted in Fig. 23. It can be seen that the computed results agree well with the given data. Thus, the proposed least-square expressions can be used to accurately and quickly compute the optimal turn-on and overlap angles from the expected torque in real time.

B. Weight Factor = 0

The fitness function is composed only of the square of rms current if the weight factor is 0. In this paper, the cubic TSF is selected. The least-square coefficients for the optimal turn-on or overlap angles can be computed from the given optimal turn-on or overlap angles for the cubic TSF when $w_f = 0$, which are obtained from the GA optimization in the last section. Table II shows the least-square coefficients in the proposed analytical expression when $N_{\rm ls}$ is equal to 6. The computed optimal turn-on and overlap angles, and the given optimal turn-on and overlap angles are illustrated in Fig. 24. It can be observed

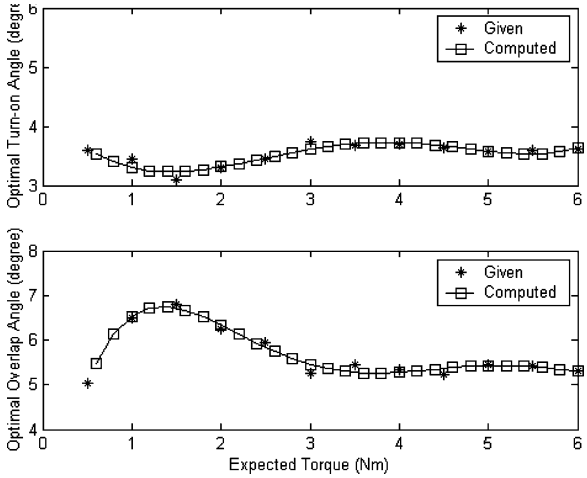

Fig. 23. Computed and given optimal turn-on and overlap angles for the exponential TSF at the weight factor of 1.0.

TABLE II
LEAST-SQUARE COEFFICIENTS FOR CUBIC TSF WHEN $w_f = 0$

Coefficient c_k	Optimal turn-on angle	Optimal overlap angle
c_0	0.600054E+01	0.557846E+01
c_1	-0.226409E-01	0.110677E+00
c_2	-0.123457E+00	0.307786E+00
c_3	-0.570895E-01	0.435182E-01
c_4	0.680853E-02	-0.279407E-01
c_5	0.460057E-02	-0.713511E-03

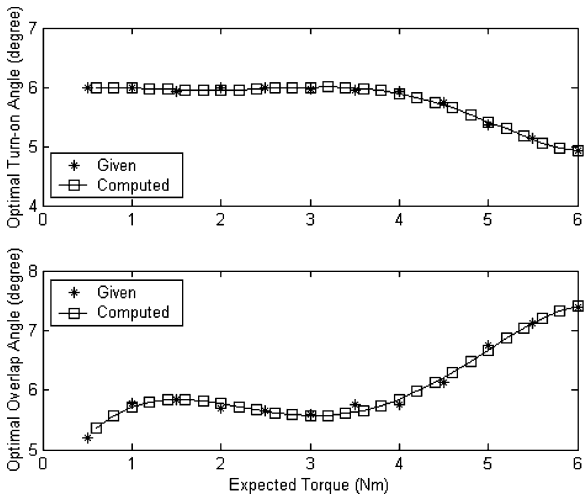

Fig. 24. Computed and given optimal turn-on and overlap angles for the cubic TSF at the weight factor of 0.

that the computed results match well with the given data. Thus, it can be used to accurately and quickly compute the optimal turn-on and overlap angles from the expected torque at real time.

TABLE III
LEAST-SQUARE COEFFICIENTS FOR SINUSOIDAL TSF WHEN $w_f = 0.5$

Coefficient c_k	Optimal turn-on angle	Optimal overlap angle
c_0	0.444060E+01	0.575410E+01
c_1	0.143490E+01	-0.248409E+00
c_2	0.101004E+00	-0.250845E+00
c_3	-0.892400E+00	0.543793E-01
c_4	-0.632626E-01	0.151270E+00
c_5	0.155682E+00	0.505087E-01
c_6	0.619797E-02	-0.170088E-01
c_7	-0.763363E-02	-0.706995E-02

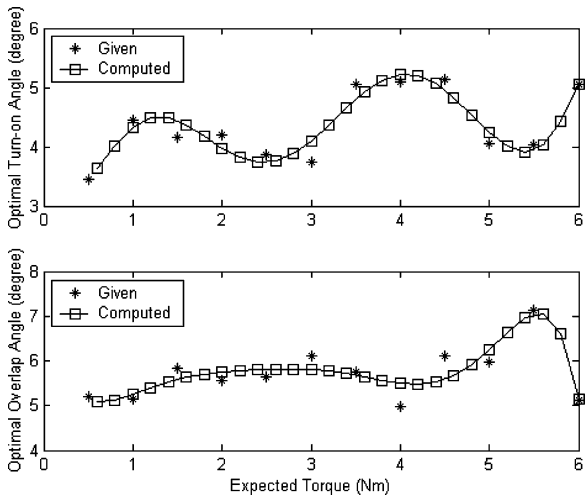

Fig. 25. Computed and given optimal turn-on and overlap angles for the sinusoidal TSF at the weight factor of 0.5.

C. Weight Factor = 0.5

When the weight factor is equal to 0.5, the fitness function consists of two optimization objectives, which are the effective rate-of-change of flux linkage and the square of rms current. If the minimum effective rate-of-change of flux linkage from the sinusoidal TSF can satisfy the requirement on the speed range, the sinusoidal TSF is a reasonable selection. In the same way, the least-square coefficients in the proposed analytical expressions can be determined from the given optimal turn-on and overlap angles, which are obtained from the GA optimization in the last section. The computed results are shown in Table III when $N_{\rm ls}$ is equal to 8. By using the analytical expressions for the optimal turn-on and overlap angles, the optimal turn-on and overlap angles at an arbitrary torque can be computed quickly. Fig. 25 shows comparisons between the computed and given results. It can be observed that the computed results are fairly consistent with the given data. Therefore, the proposed analytical expressions can be used to accurately and quickly determine the optimal turn-on and overlap angles online.

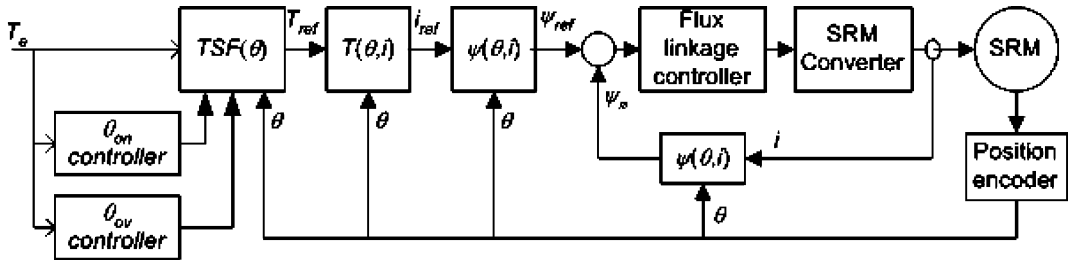

Fig. 26. Scheme of TRM control using TSFs.

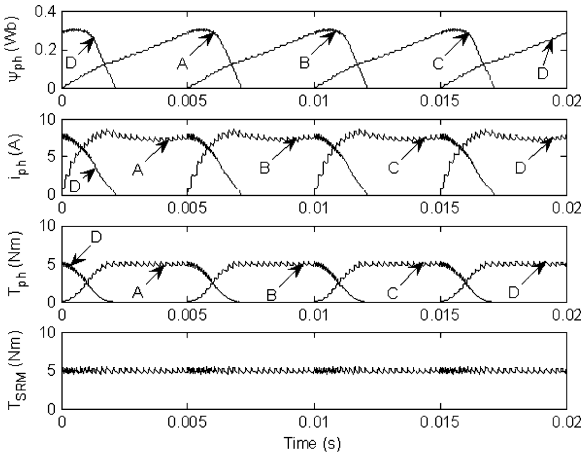

Fig. 27. TRM implemented by the sinusoidal TSF.

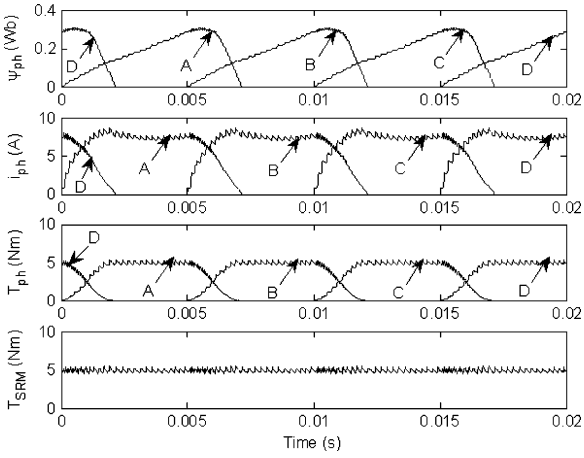

Fig. 28. TRM implemented by the cubic TSF.

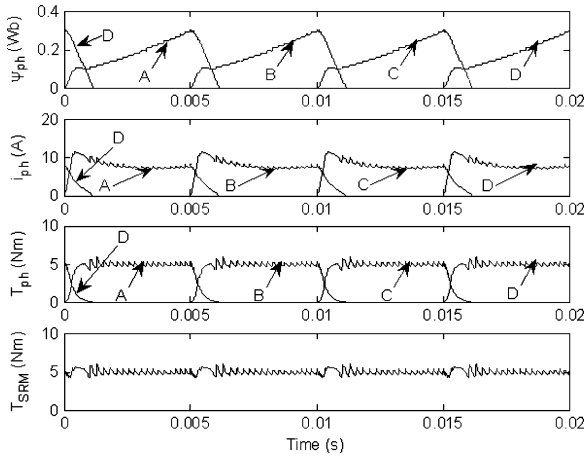

Fig. 29. TRM implemented by the exponential TSF.

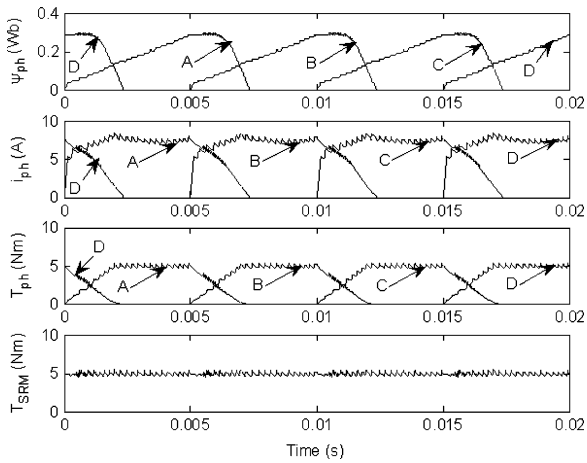

Fig. 30. TRM implemented by the linear TSF.

D. Applications

The proposed optimal TSFs are used to implement TRM in the prototype of the four-phase SRM drive by using the simulation [11], [12]. Fig. 26 illustrates the control scheme of TRM.

From the discussion in Section VIII-C, the sinusoidal TSF should be selected as the optimal TSF to implement TRM in the four-phase SRM drive if the weight factor is 0.5. Clearly, the optimization objective includes the minimization of the rate-of-change of flux linkage and the minimization of square of rms current. The optimal turn-on and overlap angles are computed based on the sinusoidal TSF, as shown in Fig. 25. The phase flux linkage, phase current, phase torque, and SRM torque profiles for four TSFs are depicted in Figs. 27–30, respectively, when the SRM drive operates at the torque of 5 Nm and the speed of 500 r/min. $\psi_{\rm ph}$ denotes the phase flux linkage, $i_{\rm ph}$ denotes the phase current, $T_{\rm ph}$ denotes the phase torque, and $T_{\rm SRM}$ denotes the SRM torque. Fig. 31 illustrates the square values of rms current from four TSFs. It can be seen that four TSFs can be used to implement TRM of the SRM drive well, and that the sinusoidal TSF results in the smaller square values of rms current than other three TSFs because the optimal TSF is selected as the sinusoidal TSF. The square values of rms current

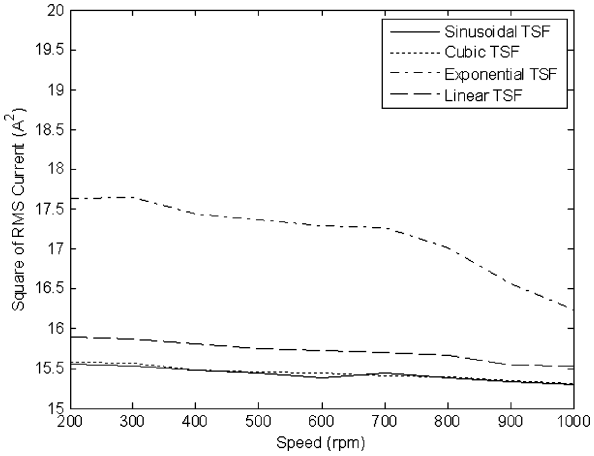

Fig. 31. Comparisons of square values of rms current between four TSFs.

for the cubic TSF are similar to the ones for the sinusoidal TSF. The square values of rms current for the exponential TSF are much larger than the ones for other three TSFs. The results of the applications are in agreement with the optimization results in the Section VII. At the same time, the maximum speed values for the sinusoidal, cubic, exponential, and linear TSFs are determined as 1360, 1350, 1710/min, and 1300 r/min. Clearly, the maximum speed for the exponential TSF is larger than other three TSFs. The maximum speed for the linear TSF is smaller than other three TSFs. The maximum speed for the sinusoidal TSF is similar to the one for the cubic TSF. Therefore, the results of the applications are consistent with the optimization results in the Section VII.

IX. Conclusion

The improved sinusoidal and exponential TSFs have been described. The investigation shows that the TSFs being used to implement TRM control are functions of turn-on angle, overlap angle, and expected torque. Large speed range and small copper loss can be found by optimizing TSFs.

GA is used to optimize the turn-on and overlap angles in order to minimize both the effective rate-of-change of flux linkage and the square of rms current. The fitness function is expressed by two optimization objectives with a weight factor to minimize the effective rate-of-change of flux linkage (maximize the speed range) and the square of rms current (minimize the copper loss). If the minimum effective rate-of-change of flux linkage (the speed range) is the only evaluating target, exponential TSF is the best selection. Cubic or sinusoidal TSFs may be the second preferred selection. On the other hand, if the minimum copper loss is the optimization target, any of the four TSFs is a reasonable selection since they all have the same minimum copper loss approximately. When the weight factor is equal to 0.5, the cubic or sinusoidal TSF is the best selection if its minimum effective rate-of-change of flux linkage can satisfy the speed range requirement. Otherwise, exponential TSF is the best selection.

The least-square polynomials are proposed to compute the optimal turn-on and overlap angles in real time. The coefficients in the analytical expressions can be determined from the given optimal turn-on and overlap angles offline. The case studies presented have shown that the developed least-square expressions can be used to accurately and rapidly compute the optimal turn-on and overlap angles from the expected torque online. The applications of the proposed optimal TSFs to the prototype of the four-phase SRM drive have demonstrated that the optimization results agree with the results of the operation of the SRM drive.

In summary, this paper provides a valuable approach to select a reasonable TSF in order to implement TRM control to realize large speed range and high operating efficiency.

Appendix

The main parameters of the prototype of the SRM drive are listed as follows:

Number of phases is 4.
Number of stator poles is 8.
Number of rotor poles is 6.
Phase resistance is 0.687 Ω.
Phase inductance is 0.0347 H when the stator pole is fully aligned with the rotor pole and the phase current is equal to 12 A.
Phase inductance is 0.00699 H when the stator pole is completely unaligned with the rotor pole and the phase current is equal to 12 A.
Phase inductance is 0.0838 H when the stator pole is fully aligned with the rotor pole and the phase current is equal to 2 A.
Phase inductance is 0.00632 H when the stator pole is completely unaligned with the rotor pole and the phase current is equal to 2 A.

References

[1] M. Illic-Spong, T. J. E. Miller, and S. R. MacMinn, "Instantaneous torque control of electric motor drives," *IEEE Trans. Power Electron.*, vol. 2, no. 1, pp. 55–61, Jan. 1987.
[2] D. S. Schramm, B. W. Williams, and T. C. Green, "Torque ripple reduction of switched reluctance motors by PWM phase current optimal profiling," in *Conf. Rec. IEEE PESC 1992*, vol. 2, pp. 857–860.
[3] I. Husain and M. Ehsani, "Torque ripple minimization in switched reluctance drives by PWM current control," *IEEE Trans. Power Electron.*, vol. 11, no. 1, pp. 83–88, Jan. 1996.
[4] S. C. Sahoo, J. X. Xu, and S. K. Panda, "Determination of current waveforms for torque ripple minimization in switched reluctance motors using iterative learning: An investigation," *IEE Proc. Electr. Power Appl.*, vol. 146, no. 4, pp. 369–377, Jul. 1999.
[5] S. K. Sahoo, S. K. Panda, and J. X. Xu, "Iterative learning-based high-performance current controller for switched reluctance motors," *IEEE Trans. Energy Convers.*, vol. 19, no. 3, pp. 491–498, Sep. 2004.
[6] S. K. Sahoo, S. K. Panda, and J. X. Xu, "Indirect torque control of switched reluctance motors using iterative learning control," *IEEE Trans. Power Electron.*, vol. 20, no. 1, pp. 200–208, Jan. 2005.
[7] X. D. Xue and K. W. E. Cheng, "A control scheme of torque ripple minimization for SRM drives based on flux linkage controller and torque sharing function," in *Proc. 2nd Int. Conf. Power Electron. Syst. Appl.*, Hong Kong, 2006, pp. 79–84.
[8] X. D. Xue, K. W. E. Cheng, and S. L. Ho, "A self-training numerical method to calculate the magnetic characteristics for switched reluctance motor drives," *IEEE Trans. Magn.*, vol. 40, no. 2, pp. 734–737, Mar. 2004.
[9] X. D. Xue, K. W. E. Cheng, S. L. Ho, and K. F. Kwok, "Trigonometry-based numerical method to compute nonlinear magnetic characteristics in switched reluctance motors," *IEEE Trans. Magn.*, vol. 43, no. 4, pp. 1845–1848, Apr. 2007.

[10] X. D. Xue, K. W. E. Cheng, and S. L. Ho, "Online and offline rotary regressive analysis of torque estimator for SRM drives," *IEEE Trans. Energy Convers.*, vol. 22, no. 4, pp. 810–818, Dec. 2007.
[11] X. D. Xue, K. W. E. Cheng, and S. L. Ho, "Simulation of switched reluctance motor drives using two-dimensional bicubic spline," *IEEE Trans. Energy Convers.*, vol. 17, no. 4, pp. 471–477, Dec. 2002.
[12] X. D. Xue, K. W. E. Cheng, and S. L. Ho, "Study of power factor in SRM drives under current hysteresis chopping control," in *Proc. 40th IEEE IAS Annu. Meeting Conf. Rec. 2005*, Oct. 2–6, vol. 4, pp. 2734–2740.

X. D. Xue received the B.Eng. degree from Hefei University of Technology, Hefei, China, in 1984, the M.Eng. degree from Tianjin University, Tianjin, China, in 1987, and the Ph.D. degree from The Hong Kong Polytechnic University, Kowloon, Hong Kong, in 2004, all in electrical engineering.

From 1987 to 2001, he was an Associate Professor in the Department of Electrical Engineering, Tianjin University, where he was engaged in teaching and research. He is currently with the Department of Electrical Engineering, The Hong Kong Polytechnic University, as a Research Fellow. He has authored or coauthored more than 70 papers. His current research interests include electrical machines, electrical drives, power electronics, electric motor drives applied to electric vehicles, and wind power generations.

K. W. E. Cheng (M'90–SM'06) received the B.Sc. and Ph.D. degrees from the University of Bath, Bath, U.K., in 1987 and 1990, respectively.

He was with Lucas Aerospace, U.K., as a Principal Engineer, where he led a number of power electronics projects. Since 1997, he has been with The Hong Kong Polytechnic University, Kowloon, Hong Kong, where he is currently a Professor and the Director of the Power Electronics Research Centre. He has authored or coauthored more than 250 papers and seven books. His current research interests include all aspects of power electronics, motor drives, electromagnetic interference (EMI), and energy saving.

Dr. Cheng received the IEE Sebastian Z. de Ferranti Premium Award in 1995, the Outstanding Consultancy Award in 2000, the Faculty Merit Award for best teaching in 2003 from the Hong Kong Polytechnic University, Faculty Engineering Industrial and Engineering Services Grant Achievement Award in 2006, and Brussels Innova Energy Gold Medal with Mention in 2007.

S. L. Ho received the B.Sc. and Ph.D. degrees in electrical engineering from the University of Warwick, Conventry, U.K., in 1976 and 1979, respectively.

During 1979, he joined The Hong Kong Polytechnic University, Kowloon, Hong Kong, where he is currently the Chair Professor in electrical utilization and the Head of Department in the Department of Electrical Engineering. He has been actively engaged in the local industry, particularly in railway engineering. He has authored or coauthored more than 100 papers in leading journals, mostly in the IEEE Transactions and Institute of Electrical Engineers (IEE) Proceedings, and holds several patents. His current research interests include traction engineering, the application of finite elements in electrical machines, phantom loading of machines, and optimization of electromagnetic devices.

Prof. Ho is a member of the Institution of Electrical Engineers of U.K. and the Hong Kong Institution of Engineers.